The Astrophysical Journal, 770:33 (14pp), 2013 June 10 doi:10.1088/0004-637X/770/1/33

ON THE FORMATION OF SILACYCLOPROPENYLIDENE (c-SiC_2H_2) AND ITS ROLE IN THE ORGANOSILICON CHEMISTRY IN THE INTERSTELLAR MEDIUM

Dorian S. N. Parker[1], Anthony V. Wilson[1], Ralf I. Kaiser[1,4], Nicholas J. Mayhall[2], Martin Head-Gordon[2,4], and Alexander G. G. M. Tielens[3,4]
[1] Department of Chemistry, University of Hawaii, Honolulu, HI 96822, USA
[2] Department of Chemistry, University of California, Berkeley, CA 94720, USA
[3] Leiden Observatory, University of Leiden, Leiden, The Netherlands
Received 2013 January 21; accepted 2013 March 20; published 2013 May 22

ABSTRACT

Organosilicon species such as silicon carbide and silicon dicarbide are considered as key molecular building blocks in the chemical evolution of the interstellar medium and are associated with the formation of silicon-carbide dust grains in the outflow of circumstellar envelopes of carbon-rich asymptotic giant branch (AGB) stars. However, the formation mechanisms of even the simplest silicon-bearing organic molecules have remained elusive for decades. Here, we demonstrate in crossed molecular beam experiments combined with ab initio calculations that the silacyclopropenylidene molecule (c-SiC_2H_2) can be synthesized in the gas phase under single-collision conditions via the reaction of the silylidyne radical (SiH) with acetylene (C_2H_2). This system denotes the simplest representative of a previously overlooked reaction class, in which the formation of an organosilicon molecule can be initiated via barrierless and exoergic reactions of silylidyne radicals with hydrocarbon molecules in circumstellar envelopes of evolved carbon stars such as IRC+10216. Since organosilicon molecules like silacyclopropenylidene can be eventually photolyzed to carbon–silicon clusters such as silicon dicarbide (c-SiC_2), silacyclopropenylidene might even represent the missing link between simple molecular precursors and silicon-carbide-rich interstellar grains.

Key words: dust, extinction – ISM: kinematics and dynamics – ISM: molecules – molecular processes

1. INTRODUCTION

During recent decades, the molecular processes involved in the formation of organosilicon molecules such as silicon carbide (SiC) and silicon dicarbide (c-SiC_2) together with their hydrogenated counterparts have received considerable attention from the astronomical (Speck et al. 1997; Ziurys 2006) and physical chemistry communities (Srinivas et al. 1991; Maier et al. 1994, 1998; Van Orden et al. 1995; Fernandez et al. 2011). This is due to the key role of silicon-bearing molecules in the chemical evolution of the interstellar medium (ISM; Ziurys 2006; Cernicharo et al. 2010) and their link to the formation of silicon-carbide dust grains in the outflow of circumstellar envelopes of carbon-rich asymptotic giant branch (AGB) stars like IRC+10216 (Jones 2001). The infrared emission feature seen in the spectra of most carbon stars at about 11.0 μm has been reliably attributed to silicon-carbide dust grains (Speck et al. 1997; Ziurys 2006). Due to the simultaneous abundance of silicon dicarbide (Thaddeus et al. 1984), organosilicon clusters are considered as key building blocks in the synthesis of more complex silicon-bearing molecules such as SiC_3 and SiC_4, which eventually lead to silicon-carbide dust grains (Ohishi et al. 1989). Sophisticated isotope analysis verified that the silicon-carbide stardust recovered from meteorites originates essentially from AGB stars with smaller portions formed in Type II supernovae and novae (Zinner 1998).

However, the basic molecular processes, which link the circumstellar silicon and carbon chemistries to grain formation, are far from being understood (Cherchneff et al. 2000; Cherchneff 2006; Decin et al. 2008). In the outer regions of carbon-rich circumstellar envelopes, where ultraviolet photons from the interstellar radiation field penetrate, astrochemical models propose that organosilicon chemistry is dictated by ion–molecule reactions, radiative associations, and dissociative recombination with either atomic or singly ionized silicon (Millar & Herbst 1994; Millar et al. 2000; Wakelam et al. 2011). In the inner regions, models assume that, starting with silicon carbide, neutral–neutral reactions of silicon–carbon clusters initiate silicon-carbide dust nucleation (Yasuda & Kozasa 2012). Further chemical growth of silicon-carbide dust is suggested to involve reactions with acetylene (C_2H_2) and the ethynyl radical (C_2H) (Yasuda & Kozasa 2012). However, the validity of these mechanisms has remained conjectural because the majority of the reactions have not been studied in the laboratory. Also, after nucleation and chemical growth in the stellar ejecta, silicon-carbide dust grains are processed in the ISM by energetic ions in prevalent shock waves (Jones et al. 1994). As sputtering by energetic ions is very efficient, the calculated lifetime of dust grains in the ISM of about 5×10^8 yr is much shorter than the injection timescale of dust by stars of 2×10^9 yr. The implication is that only a small fraction of the silicon should be in the solid state, but this contradicts observations of elemental depletions suggesting that up to 90% of silicon is depleted on grains (Tielens 1998). The prevalent notion in the field is, therefore, that chemical growth of dust is very rapid in the ISM (Draine 2009). Hence, both the inefficient formation of simple silicon-carbide clusters and the ubiquitous presence of interstellar grains suggest crucial, but hitherto unexplained, reaction pathways leading to a supply of organosilicon species via a fast chemical growth.

Here, we report the results of a crossed molecular beam experiment of the D1-silylidyne radical (SiD; $X^2\Pi$) with acetylene (C_2H_2, $X^1\Sigma_g^+$). By merging the reactive scattering data with electronic structure calculations, we furnish conclusive evidence that the silacyclopropenylidene molecule (c-SiC_2H_2) can be synthesized via a single-collision event involving the

[4] Corresponding author.

barrierless reaction of two neutral molecules: the D1-silylidyne radical and acetylene. This system denotes the simplest representative of a previously overlooked reaction class, in which the formation of an organosilicon molecule can be initiated by barrierless reactions of silylidyne radicals with unsaturated hydrocarbon molecules in circumstellar envelopes of evolved carbon stars such as IRC+10216. The experiments were conducted at a collision energy of 41 kJ mol^{-1}, which is equivalent to a temperature of about 4900 K. This is comparable to temperatures in the circumstellar envelopes of carbon-rich stars such as IRC+10216 close to the photosphere reaching temperatures up to a few thousand kelvin, thus mimicking nicely the physical (temperature) and chemical (reactant) conditions in circumstellar envelopes of carbon-rich AGB stars close to the photosphere. In the case of IRC+10216, the silylidyne (SiH) and acetylene (C_2H_2) reactants are predicted to be present at fractional abundances of up to 2×10^{-7} and 3×10^{-4}, respectively, within two stellar radii (Willacy & Cherchneff 1998). The facile route to silacyclopropenylidene and potentially more complex silicon-bearing species via silylidyne radical reactions opens up a versatile, hitherto disregarded source of silicon-bearing molecules in the ISM. Since organosilicon molecules such as silacyclopropenylidene can be eventually photolyzed to carbon–silicon clusters like c-SiC_2 (Maier et al. 1994, 1995b; Redman et al. 2003), which are considered key building blocks in interstellar grains, organosilicon molecules such as silacyclopropenylidene might even represent the missing link between simple molecular precursors and silicon-carbide-rich interstellar grains.

2. EXPERIMENTAL

The experiments were conducted under single-collision conditions in a crossed molecular beams machine (Kaiser et al. 2010). A pulsed, supersonic beam of the D1-silylidyne radical (SiD; $X^2\Pi$) at fractions of about 0.5% in the seeding gas was prepared in situ in the primary source by laser ablation of a silicon rod with 266 nm, 10–15 mJ pulses, and subsequent entrainment of the ablated silicon atoms in deuterium gas (D_2, 99.7%; Icon Isotopes Inc.). The deuterium, which was released by a piezoelectric pulsed valve (Proch-Trickl) operated at 60 Hz and a backing pressure of about 4 atm, acted as a seeding *and* a reactant gas most likely forming the D1-silylidyne radical via atomic deuterium abstraction by atomic silicon from molecular deuterium; no other silicon–deuterium-bearing molecules were present in the beam. Note that even if D1-silylidyne radicals are formed initially in the $A^2\Delta$ state, with a lifetime of only 500 ns, they decay to the ground state in the travel time of about 18 μs to the interaction region of the scattering chamber (Bauer et al. 1984). A segment of the pulsed molecular beam entraining the D1-silylidyne radicals with a well-defined peak velocity of 2555 ± 110 ms^{-1} and speed ratio of 3.3 ± 1.2 was selected using a four slit chopper wheel after passing through a skimmer. The segment of the primary beam crossed at 90° a supersonic beam of pure acetylene gas (C_2H_2; 99.99%; Matheson), which had a velocity of 900 ± 20 ms^{-1} and speed ratio of 9.2 ± 1.0, in the scattering chamber, yielding a collision energy of 41.2 ± 4.0 kJ mol^{-1}. At this collision energy, silicon atoms present in the primary beam were found not to react with acetylene. The reactive scattering signal was angularly resolved by monitoring the reaction products in 2.5 increments in the scattering plane defined by the primary and secondary beams at distinct mass-to-charge ratios using a triply differentially pumped quadrupole mass spectrometer (QMS) in the time-of-flight (TOF) mode after electron-impact ionization of the neutral molecules at 80 eV. The QMS acts as a mass filter only allowing ions with the selected mass-to-charge, m/z, value to pass through to the detector. The ions with the selected mass-to-charge upon exiting the QMS are accelerated toward a high-voltage (−22.5 kV) stainless steel target coated with an aluminum layer, which upon impact initiates an electron cascade. The electron cascade gets accelerated away from the stainless steel target and toward an aluminum-coated organic scintillator, which creates a photon cascade that is detected by a photomultiplier tube (PMT). The signal from the PMT was filtered by a discriminator set at 1.6 mV to reduce background noise before being recorded by a multichannel scaler, which records the signal in a series of "time bins" to obtain the TOF spectra. The laboratory angular distribution was obtained by integrating the TOF spectra and scaling for the data accumulation time at each angle. In order to obtain the information about the reaction dynamics, the laboratory data (TOF spectra and product angular distribution) were fit with Legendre polynomials that were converted from the laboratory frame to the center-of-mass (CM) reference frame using a forward convolution technique yielding the CM translational energy, $P(E_T)$, and the angular flux distributions, $T(\theta)$ (Vernon 1981; Weis 1986). The fitting procedure entails making an initial prediction of the product translational energy $P(E_T)$ and the angular distribution $T(\theta)$ in the CM reference frame and iteratively optimizing them until the laboratory frame data can be accurately matched.

3. THEORETICAL METHODS

Molecular structures were obtained via B3LYP/6-311+G** geometry optimizations and frequency calculations. All geometric stationary points were characterized by frequency calculations to ensure that geometric minima had zero imaginary frequencies and that transition states had exactly one imaginary frequency. Harmonic zero-point energy corrections were also computed at the B3LYP/6-311+G** level. Single-point energy evaluations were then computed at the CCSD(T)/aug-cc-pVTZ level of theory (Pople et al. 1987; Dunning 1989), employing the frozen core approximation. Except where otherwise specified, all energies are computed at the CCSD(T)/aug-cc-pVTZ//B3LYP/6-311+G** level of theory. To compare directly to the experimental data, reaction energies leading to [p1] to [p3] were computed via

$$E(\mathrm{CCSD(T)/CBS}) = E(\mathrm{HF/aug\text{-}cc\text{-}pV5Z}) + E^{\mathrm{corr}}(\mathrm{MP2/CBS_{4,5}}) + E^{\mathrm{corr}}(\mathrm{CCSD(T)/aug\text{-}cc\text{-}pV4Z}) - E^{\mathrm{corr}}(\mathrm{MP2/aug\text{-}cc\text{-}pV4Z}) + \mathrm{ZPE(B3LYP/4z)},$$

where $E^{\mathrm{corr}}(\mathrm{MP2/CBS_{4,5}})$ is the extrapolated MP2 correlation energy using the aug-cc-pV4Z and aug-cc-pV5Z basis sets and the extrapolation approach (Halkier et al. 1998):

$$E^{\mathrm{corr}}(\mathrm{MP2/CBS}_{M,N}) = [N^3 E^{\mathrm{corr}}(\mathrm{MP2/aug\text{-}cc\text{-}pVNZ}) - M^3 E^{\mathrm{corr}}(\mathrm{MP2/aug\text{-}cc\text{-}pVMZ})]/[N^3 - M^3],$$

where M and N denote the cardinal number, X, for the aug-cc-pVXZ basis sets. These CCSD(T)/CBS results are observed to be converged to within 3 kJ mol^{-1}. To confirm that no entrance barrier exists for the reaction of D1-silylidyne with acetylene, a steepest descent optimization was performed starting from separated reactants. The energies are plotted in Figure 4. All calculations were performed with the QChem suite of electronic structure programs (Kong et al. 2000).

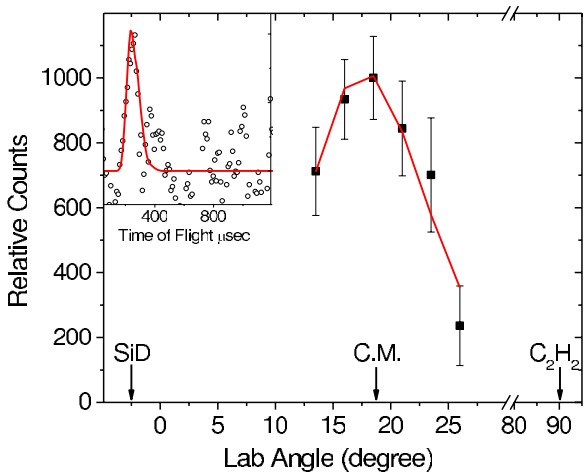

Figure 1. Laboratory angular distribution at mass-to-charge (m/z) of 54 (c-$SiC_2H_2^+$) recorded in the reaction of the D1-silylidyne radical with acetylene. Closed squares indicate experimental data and the solid red line the calculated distribution with the best-fit center-of-mass functions as depicted in Figure 2. C.M. designates the center-of-mass angle. Inset shows time-of-flight spectrum recorded at the center-of-mass angle, with open circles representing experimental data and the solid red line as the best fit.

4. RESULTS

4.1. Crossed Molecular Beams Studies: Laboratory Frame

The reaction of the D1-silylidyne radical (SiD; $X^2\Pi$) with acetylene (C_2H_2, $X^1\Sigma_g^+$) was probed under single-collision conditions in the gas phase exploiting the crossed molecular beam approach. After intersecting a supersonic beam of D1-silylidyne with acetylene perpendicularly at a collision energy of 41.2 ± 4.0 kJ mol^{-1}, the neutral reaction products underwent electron impact ionization at 80 eV within a triply differentially pumped quadrupole mass spectrometric detector and were subsequently mass- and velocity-analyzed to record TOF spectra at well-defined mass-to-charge ratios at distinct laboratory angles. For the D1-silylidyne–acetylene system, we attempted to monitor reactive scattering signal at mass-to-charge ratios of $m/z = 55$ (SiC_2HD^+), $m/z = 54$ ($SiC_2H_2^+/SiC_2D^+$), and $m/z = 53$ (SiC_2H^+). The reaction of D1-silylidyne (SiD; 30 amu) with acetylene (C_2H_2; 26 amu) did not result in reactive scattering signal at $m/z = 55$ (SiC_2HD^+). Therefore, we conclude that under single-collision conditions, this reaction does not lead to the formation of SiC_2HD (55 amu) via atomic hydrogen loss (1 amu). Reactive scattering signal was observed at $m/z = 54$ (Figure 1). Considering the molecular formula and molecular weight of the reactants, signal at $m/z = 54$ can originate from two channels: SiC_2H_2 (54 amu) plus atomic deuterium (D; 2 amu) or SiC_2D (54 amu) together with molecular hydrogen (H_2; 2 amu). We also attempted to monitor reactive scattering signal at $m/z = 53$ (SiC_2H) formed via HD (3 amu) elimination, but were unsuccessful. Therefore, the interpretation of the raw data alone indicates a formation of the organosilicon molecule(s) SiC_2H_2 and/or SiC_2D via a single-collision event of two neutral reactants. Further, we can conclude that the atomic hydrogen (H) and the hydrogen deuteride (HD) elimination leading to SiC_2DH (55 amu) and SiC_2H (53 amu), respectively, are closed under our experimental conditions.

4.2. Crossed Molecular Beams Studies: Center-of-Mass Frame

After identifying the SiC_2H_2 and/or SiC_2D reaction products, we will now transform the experimental data from the laboratory to the CM reference frame (Kaiser et al. 2010). This procedure allows first an assignment of the reaction product(s); recall that based on the raw data alone, both SiC_2H_2 and SiC_2D can contribute to signal at $m/z = 54$. Once the product(s) is (are) characterized, we can expose the underlying chemical dynamics leading to the formation of the organosilicon molecule(s). Best fits of the laboratory data are overlaid in Figure 1 with the CM angular ($T(\theta)$) and translational flux distributions ($P(E_T)$) depicted in Figure 2. The laboratory data could be fit with a single-reaction channel of reaction products with molecular masses 54 amu (SiC_2H_2, SiC_2D) and 2 amu (D, H_2). A closer look at the CM functions provides important information on the pertinent reaction channel(s) and dynamics. Let us analyze the CM translational distribution first, since the $P(E_T)$ assists in the assignment of the product isomer(s). For those reaction products formed without internal excitation, the high-energy cutoff of the $P(E_T)$ of 54 ± 4 kJ mol^{-1} represents the sum of the reaction exoergicity plus the collision energy (41.2 ± 4.0 kJ mol^{-1}). A subtraction of the collision energy indicates that the reaction is slightly exoergic by 13 ± 8 kJ mol^{-1}. This value is in very good agreement with our computed value for an exoergic reaction of 10 kJ mol^{-1} to form the silacyclopropenylidene molecule (c-SiC_2H_2) plus atomic deuterium (Figure 3). The energetics cannot account for the formation of SiC_2D plus molecular hydrogen; here, the computed exoergicities of this channel of 32 kJ mol^{-1} and 61 kJ mol^{-1} to form the cyclic and linear SiC_2D isomers, respectively, do not match the experimental data. Therefore, we can conclude that the silacyclopropenylidene molecule (c-SiC_2H_2) is formed in the reaction of the D1-silylidyne radical with acetylene. Further, the translational energy distribution is closely peaked at zero translational energy; the laboratory data could be fit with a broad plateau from 0 up to about 8 kJ mol^{-1}. These findings suggest that the exit

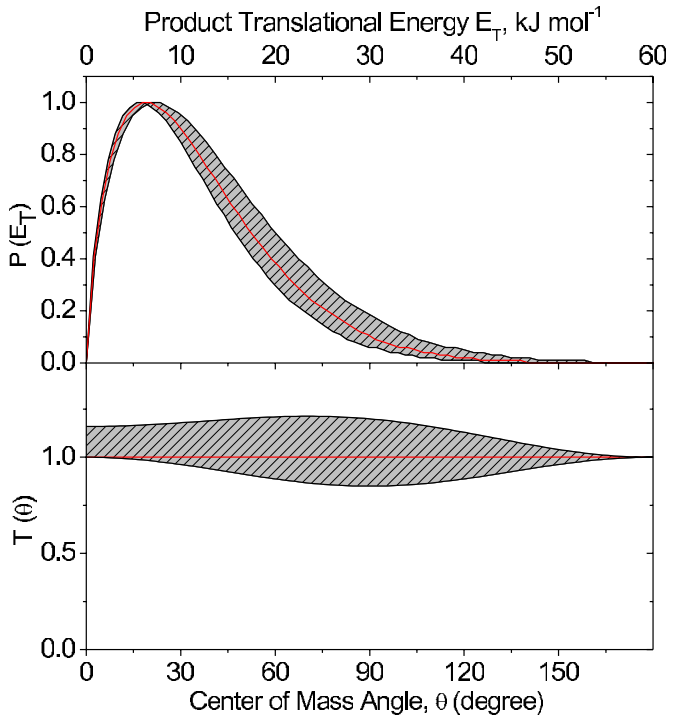

Figure 2. Center-of-mass angular (top) and translational energy flux distributions (bottom) leading to the formation of the silacyclopropenylidene (c-SiC_2H_2) plus atomic deuterium in the reaction of the D1-silylidyne radical with acetylene. Hatched areas indicate the acceptable upper and lower error limits of the fits. The solid red lines define the best-fit function.

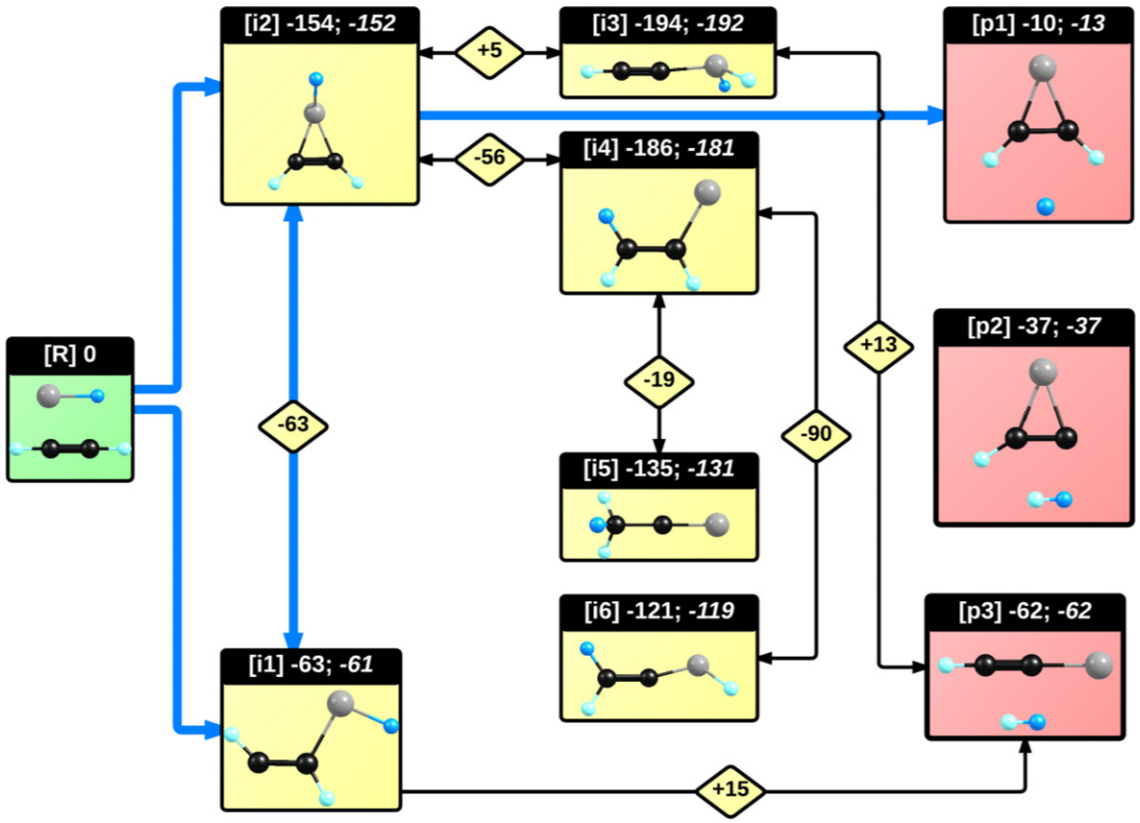

Figure 3. Flow diagram of the reaction of the D1-silylidyne radical (SiD) with acetylene (C_2H_2) including reaction pathways energetically accessible in the crossed molecular beam experiments. Relative energies are given in units of kJ mol^{-1}. The energetics in italics are given for the reaction of the silylidyne radical (SiH) with acetylene (C_2H_2). Energies of the transition states are denoted with diamonds. Carbon, silicon, hydrogen, and deuterium atoms are defined in black, silver, light blue, and dark blue, respectively. Optimized Cartesian coordinates for all structures are given in Figure 4 and Tables 3 and 4. The elucidated reaction mechanism is highlighted in blue.

transition state to form silacyclopropenylidene plus atomic deuterium is rather loose. Finally, the energy channeled on average into the translational degrees of freedom of the final products is only 26% ± 5%; this order of magnitude suggests indirect scattering dynamics involving the unimolecular decomposition of a $SiDC_2H_2$ complex. The indirect nature of the reaction mechanism is also confirmed by the CM angular distribution. Here, the $T(\theta)$ depicts intensity over the complete angular range as indicative of an indirect, complex forming reaction mechanism. Also, the CM angular distribution could be fit within the error limits with slightly forward scattered or forward–backward symmetric distributions. These findings propose that the lifetime of the decomposing intermediate might be close to its rotational period (slightly forward scattered) or that the lifetime of the decomposing $SiDC_2H_2$ intermediate is longer than its rotational period (forward–backward symmetric). Note that no conclusive evidence exists to determine whether the distribution holds a pronounced peak or dip at 90°; an isotropic (flat) distribution leads to an acceptable fit of the experimental data.

4.3. Electronic Structure Calculations: Reaction Intermediates

The electronic structure calculations were performed at a level of theory high enough to predict relative energies of the local minima within 10 kJ mol^{-1} and reaction energies to a precision of 3 kJ mol^{-1} (Figure 4 and Tables 3 and 4). In contrast to the well-characterized SiC_2H_2 potential energy surface (PES; Vacek et al. 1991; Maier et al. 1995a, 1995b; Draine 2009), the investigation of the SiC_2H_3 PES is in its infancy; therefore, we conducted a complete theoretical study of the surface. Our

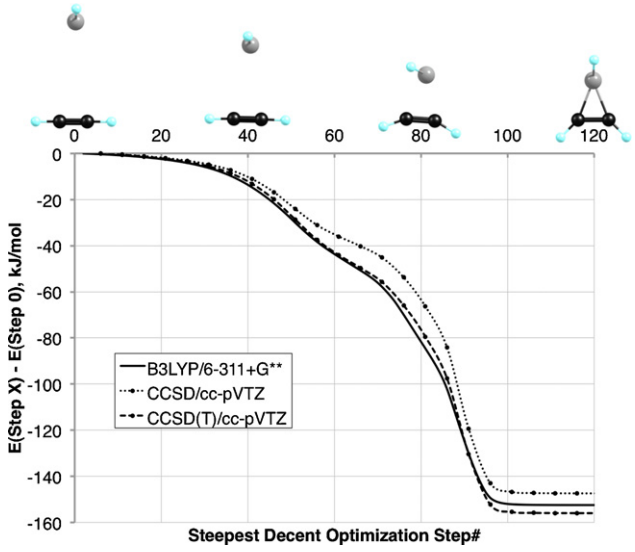

Figure 4. Steepest descent path for the reaction of the silylidyne radical with acetylene. The structures are shown for geometry steps 0, 40, 80, and 120. The B3LYP/6-311+G** method was used to obtain a steepest descent path, and CCSD/cc-pVTZ and CCSD(T)/cc-pVTZ single-point energies were computed to verify that a barrierless path exists that connects the separated reactants and intermediate [i2].

(A color version of this figure is available in the online journal.)

ab initio calculations suggest the existence of six SiC_2H_2D reaction intermediates [i1] to [i6] and nine reaction products, of which only three—[p1] to [p3]—are energetically accessible under our experimental conditions (Figure 3 and Tables 1, 2, 3,

Table 1
Reaction Products (p1 to p9) Formed via the Unimolecular Decomposition of Intermediates ([i1] to [i6]) via Atomic (H/D) and Molecular "Hydrogen" (H_2/HD) Loss Pathways; Primed Products Represent Isotopologues

	H	D	H_2	HD
[i1] 				
-63; *-61* ($C_1 - {}^2A$)	+70; *+71* (p5'; $C_s - {}^1A'$)	…	+134; *+135* (p8'; $C_s - {}^2A'$)	-62*; *-62** (p3; $C_{\infty v}$ - $^2\Pi$)
[i2] 	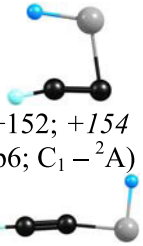			
-154; *-152* ($C_s - {}^2A'$)	+70; *+71* (p5'; $C_s - {}^1A'$)	-10*; *-13** (p1; $C_{2v} - {}^1A_1$)	+122; *+123* (p9; $C_1 - {}^2A$)	-37*; *-37** (p2; $C_1 - {}^2A$)
[i3] 	 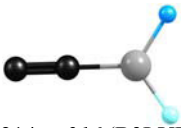			 
-194; *-192* ($C_s - {}^2A_1$)	+214; *+216* (B3LYP) (p7; $C_s - {}^1A'$)	+74; *+71* (p5; $C_s - {}^1A'$)	+134; *+135* (p8'; $C_s - {}^2A'$)	-62*; *-62** (p3; $C_{\infty v} - {}^2\Pi$) +135; *+135* (p8; $C_s - {}^2A'$)
[i4] 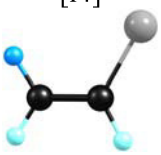	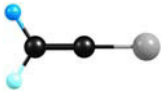			
-186; *-181* ($C_1 - {}^2A$)	+60; *+64* (p4'; $C_s - {}^1A'$)	…	-66*; *-61** (p3'; $C_{\infty v}$ - $^2\Pi$)	…
[i5] 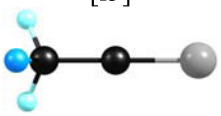	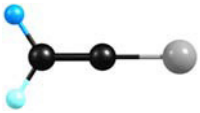			
-135; *-131* ($C_{3v} - {}^2A_1$)	+60; *+64* (p4'; $C_s - {}^1A'$)	+67; *+64* (p4; $C_s - {}^1A'$)	-66*; *-62** (p3'; $C_{\infty v}$ - $^2\Pi$)	-62*; *-62** (p3; $C_{\infty v}$ - $^2\Pi$)
[i6] 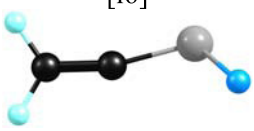				
-119; *-117* ($C_1 - {}^2A$)	+70; *+71* (p5'; $C_s - {}^1A'$)	+67; *+64* (p4; $C_s - {}^1A'$)	+134; *+135* (p8'; $C_s - {}^2A'$)	+135; *+135* (p8; $C_s - {}^2A'$)

Notes. The overall reaction energies are given in kJ mol^{-1} with respect to the separated D1-silylidyne radical (SiD) and acetylene (C_2H_2) reactants. Energies in italics are given for the reaction of the silylidyne radical (SiH) with acetylene (C_2H_2); energies marked with "*" are obtained from CCSD(T)/CBS calculations. The point groups and symmetries of the electronic wave functions are included in parentheses. Black: carbon; silver: silicon; light blue: hydrogen; dark blue: deuterium.

Table 2
Structures for [i7], [p10], and [p11]

[i7]	[p10]	[p11]
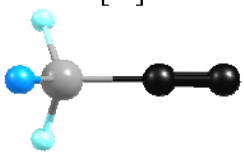		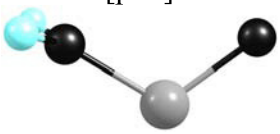
+45; *+48* (C_{3v} – ^{2}A1)	+193; +195 (C_{2v} – ^{1}A1)	+480; +477 (B3LYP) (C_s – ^{1}A')
[i1a]	[i1b]	[i1c]
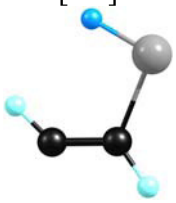	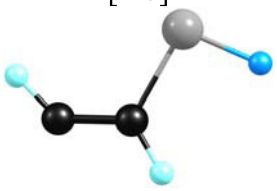	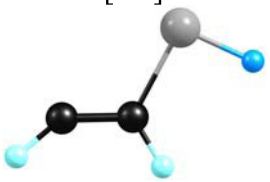
-63; *-61* (C_1 – ^{2}A)	-56; *-55* (C_1 – ^{2}A)	-49; *-48* (C_1 – ^{2}A)

Note. The different conformational isomers [i1a], [i1b], and [i1c] are also provided.

and 4). The D1-silylidyne radical (SiD; $X^2\Pi$) is predicted to add without entrance barrier to the carbon–carbon triple bond of acetylene (C_2H_2, $X^1\Sigma_g^+$) to one or two carbon atoms yielding the collision complexes [i1] and [i2], respectively, which are stabilized by −63 and −154 kJ mol^{-1} with respect to the separated reactants (Figure 4). The absence of an entrance energy barrier has been confirmed by a careful scan of the PES in the entrance channel. Our calculations clearly depict that the reaction has no entrance barrier; here, the potential energy of the system steadily and monotonically decreases as the D1-silylidyne radical approaches acetylene. The D1-1-sila-1-propene-1,3-diylidene intermediate [i1] undergoes a de facto barrierless ring closure to the D1-1-silacyclopropenyl radical [i2]. The latter can isomerize, via a hydrogen shift from the carbon to the silicon atom followed by a simultaneous ring opening to intermediate [i3] via a barrier located 5 kJ mol^{-1} above the energy of the separated reactants. The D1-1-silapropargyl radical [i3] represents the global minimum of the doublet SiC_2H_2D PES and resides in a deep potential energy well of −194 kJ mol^{-1}. Compared to the [i2] ↔ [i3] isomerization, [i2] rearranges preferentially to the D1-ethynylsilylidyne intermediate [i4] via a silicon-to-carbon deuterium migration and ring opening, since this pathway involves a lower barrier located only 98 kJ mol^{-1} above intermediate [i2]. Intermediate [i4] is connected to the SiC_2H_2D isomers [i5] (D1-1-sila-1-propyn-1-yl) and [i6] (D1-3-silapropargyl) through C1–C2 and C2–Si hydrogen shifts, respectively. What is the fate of these isomers? Intermediate [i5] can only isomerize back to [i4]; although [i5] is accessible from [i6], the transition state is located 55 kJ mol^{-1} above the separated reactants and hence cannot be overcome considering a collision energy in our experiments of only 41.2 ± 4.0 kJ mol^{-1}. Likewise, intermediate [i6] can only isomerize back to its precursor [i4]; an alternative reaction pathway from [i6] to [i1] is less favorable since the transition state is located 38 kJ mol^{-1} above the energy of the separated reactants.

Having discussed the addition pathways and consecutive isomerizations, we would like to address briefly potential insertion and abstraction routes. Here, we could not locate any reaction pathway leading to an insertion of the D1-silylidyne radical into the acetylenic carbon–hydrogen bond. Also, the D1-silylidyne radical cannot abstract a hydrogen atom from acetylene-forming ethynyl (C_2H, $X^2\Sigma^+$) plus D1-silylene (SiHD, X^1 A'); this reaction is endoergic by 195 kJ mol^{-1} and hence closed under our experimental conditions. In summary, our electronic structure calculations reveal that the reaction of the D1-silylidyne radical (SiD; $X^2\Pi$) with acetylene (C_2H_2, $X^1\Sigma_g^+$) is initiated by a barrierless addition yielding collision complexes [i1] and/or [i2], which have the possibility of further isomerization to access [i3] to [i6] as summarized in Figure 3. The fact that the D1-silylidyne radical addition to acetylene is barrierless is consistent with previous CASSCF calculations that predicted barrierless addition of both ground- (Si(^3P)) and excited-state silicon atoms (Si(^1D)) to acetylene (Su et al. 1990; Talbi 2005).

4.4. Electronic Structure Calculations: Reaction Products

The electronic structure calculations also provide fundamental insight into the reaction products formed via unimolecular decomposition of intermediates [i1] to [i6] via *atomic* (H/D) and *molecular* (H_2/HD) hydrogen elimination. Our ab initio calculations expose nine isotopomers and isotopologues, which can be formed by atomic hydrogen and deuterium loss (Table 1); exoergic reaction channels are included in Figure 3. Combining the electronic structure calculations with the experimental observations delivers a sophisticated understanding of the unimolecular dynamics that goes beyond what can be obtained from our static electronic structure calculations alone.

Let us focus our attention first on the atomic hydrogen loss channel. The reaction energies (Table 1) indicate that all atomic hydrogen loss pathways are endoergic by at least 60 kJ mol^{-1}; these energies are well above the collision energy of the crossed molecular beam study of 41.2 ± 4.0 kJ mol^{-1}. We therefore have to conclude that the atomic hydrogen loss channel is closed in

Table 3
Optimized Cartesian Coordinates in Angstroms for the Reactants, Transition States, and Products Compiled in Figure 3

Species (Energy)	Atom	x (Å)	(y) (Å)	z (Å)
Reactants				
C_2H_2 (−77.3566503)	C	0	0	−0.5997
	H	0	0	−1.6629
	C	0	0	0.59966
	H	0	0	1.66287
SiH (−290.0138302)	Si	0	0	−0.1023
	H	0	0	1.43212
Intermediates				
[i1a] (−367.3979782)	C	1.551904	−0.360623	0.09047
	C	0.693987	0.611207	−0.116
	Si	−1.082424	−0.020371	0.04334
	H	0.937974	1.665765	−0.0071
	H	1.545535	−1.437888	−0.0235
	H	−0.804915	−1.44619	−0.4229
[i1b] (−367.3939413)	C	1.702343	−0.251262	0.00162
	C	0.664567	0.556032	−0.002
	Si	−1.074167	−0.232218	−0.0006
	H	1.845514	−1.326187	0.00165
	H	0.803747	1.638352	−0.0014
	H	−1.812376	1.110265	0.01063
[i1c] (−367.3911725)	C	1.663543	−0.358189	0
	C	0.653	0.47848	0
	Si	−1.121466	−0.220335	0
	H	0.836795	1.560996	0
	H	−1.782577	1.163039	0
	H	2.747052	−0.361083	0
[i2] (−367.4295161)	C	0.855989	0.026456	−0.6693
	H	1.613302	0.092157	−1.4423
	C	0.855989	0.026456	0.66932
	H	1.613302	0.092157	1.44226
	Si	−0.839541	−0.113979	0
	H	−1.744894	1.093915	0
[i3] (−367.4425538)	C	0.70792	−0.000125	−0.0392
	H	−1.681515	1.234112	−0.4932
	C	1.920733	0.000029	−0.0075
	H	2.984931	0.000149	−0.0031
	Si	−1.09954	0.000018	0.0907
	H	−1.681772	−1.23394	−0.4932
[i4] (−367.4473961)	C	0.513241	0.549323	0.06327
	H	0.735734	1.612325	−0.0456
	C	1.552416	−0.315293	−0.0044
	H	2.569676	0.007448	−0.2143
	Si	−1.22235	−0.116911	−0.0152
	H	1.413545	−1.387204	0.12022
[i5] (−367.4286848)	C	0.324863	−0.00157	−0.0163
	H	2.208839	0.871272	−0.5148
	C	1.780841	−0.000629	−0.0043
	H	2.21454	−0.913218	−0.4312
	Si	−1.370084	0.000193	0.00208
	H	2.123579	0.052432	1.04073
[i6] (−367.4234814)	C	1.826836	−0.021682	0.02182
	H	2.499303	0.724843	−0.402
	C	0.525694	0.116942	−0.0466
	H	−1.617236	1.212151	0.58595
	Si	−1.235601	−0.116938	−0.0392
	H	2.301159	−0.871431	0.51359
Transition States				
[i2–i4] (−367.3922625)	C	0.773153	0.70224	0.06908
	H	1.197314	1.689774	−0.0394
	C	1.159384	−0.511906	−0.0212
	H	1.872839	−1.28709	−0.2312
	Si	−1.021625	−0.014147	−0.0327
	H	−0.362625	−1.346637	0.44088
[i2–i1a] (−367.3961103)	C	1.360025	−0.464656	0.09079
	H	1.117326	1.679495	−0.0682
	C	0.77556	0.651375	−0.1228
	H	1.511009	−1.522953	0.1059
	Si	−1.036985	−0.003387	0.06984
	H	−0.924052	−1.229431	−0.8234
[i2–i1c] (−367.3900938)	C	−1.518721	0.40154	−0.0487
	H	−2.531497	0.67158	−0.3124
	C	−0.667451	−0.571101	0.12625
	H	−0.920948	−1.634753	0.06358
	Si	1.066792	0.210225	0.03992
	H	1.63439	−0.962609	−0.7752
[i2–i3] (−367.3684117)	C	−0.650858	0.088024	0.04123
	H	0.073918	−0.583515	−1.0366
	C	−1.893286	0.009485	0.03266
	H	−2.956167	−0.048582	0.00267
	Si	1.195048	−0.091749	0.07101
	H	1.416438	1.331533	−0.4034
[i4–i6] (−367.4087909)	C	0.475972	−0.05942	−0.0317
	H	−0.526016	1.276111	0.38523
	C	1.802382	−0.014454	−0.0024
	H	2.365321	0.871866	−0.2807
	Si	−1.277305	−0.058316	−0.0146
	H	2.372847	−0.888307	0.30426
[i4–i5] (−367.3792461)	C	0.378435	−0.004073	0.05997
	H	2.373443	0.855781	0.29153
	C	1.785397	−0.030807	0.05739
	H	0.899877	0.405028	−0.9683
	Si	−1.328418	−0.007899	0.00988
	H	2.341538	−0.940946	−0.1656
[i3–i6]* (−367.3400746)	C	1.324076	0.292117	−0.0379
	H	2.191754	0.911573	−0.1894
	C	0.728701	−0.831723	0.04059
	H	−1.327795	−0.088089	−1.368
	Si	−0.959752	0.083256	0.09826
	H	0.255908	1.248567	0.16543
[i6–i1]* (−367.3550194)	C	1.879788	−0.088156	0.02432
	H	1.072434	0.929633	−0.597
	C	0.617779	0.02514	0.03172
	H	−1.399037	1.333549	0.41039
	Si	−1.256995	−0.12444	−0.0215
	H	2.939126	−0.142923	0.15121
[i6–i5]* (−367.3488209)	C	−1.161052	−0.31483	−0.0002
	H	−1.683975	−0.636215	−0.9063
	C	−0.546217	0.978753	0.00024
	H	−0.136982	−1.36908	−0.0003
	Si	0.981763	−0.095746	−0.0001
	H	−1.680106	−0.637792	0.90776
[i2–p2]* (−367.3322051)	C	1.020116	0.501718	0.15142
	H	1.530734	1.432425	0.33392
	C	1.072597	−0.719433	−0.2294
	H	−0.281784	−1.404799	0.41934
	Si	−0.912801	0.178251	−0.0861
	H	−1.02601	−1.216849	0.92056
[i1b–p3] (−367.3622466)	C	1.898015	0.06855	0
	H	2.954584	0.197378	4E−06
	C	0.680829	−0.068582	−1E−06

Table 3
(Continued)

Species (Energy)	Atom	x (Å)	(y) (Å)	z (Å)
	H	−0.113989	−1.15979	1E−06
	Si	−1.222697	0.172422	0
	H	−1.195894	−1.451302	0
[i3–p3] (−367.3624500)	C	0.697041	0.052826	0.02465
	H	−1.200146	1.330987	−0.5802
	C	1.911712	0.007304	0.00356
	H	2.976063	0.004441	0.00101
	Si	−1.123292	−0.198364	−0.0179
	H	−1.702341	1.080883	0.66105
[i5–p3]* (−367.3353666)	C	0.352047	−0.032922	0.00046
	H	2.405474	0.968438	0.42226
	C	1.639362	−0.19367	0.00071
	H	2.406043	0.971116	−0.4233
	Si	−1.370935	0.024042	−0.0002
	H	2.433119	−0.916585	−0.0034
Products				
[p1] (−366.8629939)	C	0.799862	−0.00004	−0.6704
	H	1.56145	0.000168	−1.4431
	C	0.799862	−0.00004	0.67041
	H	1.56145	0.000168	1.44308
	Si	−0.908661	0.000011	0
[p2] (−366.1963346)	C	0.997387	0.440108	1E−06
	H	1.727378	1.237674	−3E−06
	C	0.748015	−0.838908	0
	Si	−0.871413	0.082509	0
[p3] (−366.2107580)	C	0	0	−1.8062
	H	0	0	−2.8709
	C	0	0	−0.5808
	Si	0	0	1.22807
Higher Energy Structures				
[i7]* (−367.3696690)	C	0	0	0.87504
	H	1.402059	0	−1.4402
	C	0	0	2.0906
	H	−0.70103	1.214219	−1.4402
	Si	0	0	−0.9624
	H	−0.70103	−1.214219	−1.4402
[p6]∗ (−366.7946399)	C	0.838624	−0.825131	−0.0002
	H	1.671143	1.338236	6.9E−05
	C	1.16748	0.393319	0.00013
	H	−0.714731	1.513299	−0.0008
	Si	−0.928074	−0.018619	0.00006
[p10]* (−366.7729703)	C	0.627479	0	−1.0446
	H	0	−1.204754	1.53688
	C	−0.627479	0	−1.0446
	H	0	1.204754	1.53688
	Si	0	0	0.67578
[p4]* (−366.8387851)	C	0.430948	0.000002	0
	H	2.337495	0.921776	0
	C	1.753198	−0.000001	0
	H	2.337489	−0.921781	0
	Si	−1.26999	0	0
[p5]* (−366.8299141)	C	0.649322	−0.054635	0
	H	2.929692	0.031	0
	C	1.865133	0.00724	0
	H	−1.430351	−1.388996	0
	Si	−1.184719	0.117312	0
[p7]* (−366.7767606)	C	0.000001	0	2.02451
	H	1.23094	0	−1.7546
	C	−0.000001	0	0.75251
	H	−1.230939	0	−1.7546
	Si	0	0	−0.9395
[p11]* (−366.6805914)	C	−1.36761	0.31429	0
	H	−1.911952	0.526775	−0.9164
	C	1.5374	0.645987	0
	Si	0.200369	−0.486801	0
	H	−1.911952	0.526775	0.91639
[p9]* (−366.129622)	C	0.953084	0.654739	−0.0021
	H	−1.668944	0.239686	−1.0418
	C	1.04204	−0.601013	−0.0892
	Si	−0.735843	−0.040146	0.11352
[p8]* (−366.136105)	C	0.687981	0.083671	0
	H	−1.818168	1.14909	0
	C	1.966654	0.004472	0
	Si	−1.007831	−0.119853	0

Notes. B3LYP/6-311+G** energies in hartrees are given in parentheses. Structures [i1a], [i1b], and [i1c] are conformational isomers (as shown in Table 2), which have very small isomerization barriers of less than 5 kJ mol^{-1}. Symbol "*" shows energetically not accessible under our experimental conditions.

the reaction of the D1-silylidyne radical with acetylene. This conclusion correlates well with our experimental finding suggesting that within the detection limits of our system, no atomic hydrogen loss was observed. With respect to the atomic deuterium elimination, the ab initio calculations predict that only the formation of silacyclopropenylidene [p1] is exoergic by 10 kJ mol^{-1} with respect to the separated reactants. This finding agrees nicely with our experimental finding indicating a reaction exoergicity of 13 ± 8 kJ mol^{-1} for the atomic deuterium loss channel. The ab initio calculations predict that silacyclopropenylidene [p1] is formed through the unimolecular decomposition of D1-silacyclopropenyl [i2] via a loose exit transition state. Further, we would like to briefly address potential isotope scrambling. Figure 3 shows that intermediates [i3] to [i6] have a hydrogen and deuterium atom connected to the same heavy atom, which would provide an opportunity for isotope scrambling in [i2], if intermediates [i3] to [i6] were involved in the reaction and if the system behaved statistically, i.e., the rate of vibrational energy redistribution is fast compared to the unimolecular decomposition timescale. The experimental lack of signal at $m/z = 55$ rules out any atomic hydrogen loss suggesting a non-statistical vibrational energy redistribution. Activation of the silicon-deuterium bond apparently leads preferentially to dissociation rather than isomerization, which requires more concerted motion.

Finally, we will address the molecular hydrogen loss pathway leading to SiC_2D isomer(s) (54 amu). Based on the reaction energies (Table 1), only intermediates [i4] and [i5] can undergo unimolecular decomposition via molecular hydrogen (H_2) elimination forming the D1-silapropenylidyne radical [p3]; the overall reaction exoergicity was computed to be 62 kJ mol^{-1}. However, the ab initio calculations suggest that no reaction pathway exists connecting [i4] or [i5] to the D1-silapropenylidyne radical [p3] plus molecular hydrogen. A transition state could be located for the molecular hydrogen loss from intermediate [i5]. Nevertheless, this transition state lies 103 kJ mol^{-1} above the energy of the separated reactants and hence is energetically not accessible under our experimental conditions.

Table 4
Vibrational Frequencies for the Molecular Species Investigated in the Present Study

Species	No Deuterium (cm^{-1})	Deuterated (cm^{-1})		
		Reactants		
C_2H_2	H			
	657.45			
	657.45			
	773.94			
	773.94			
	2062.56			
	3419.4			
	3522.15			
SiH	H	D(2)		
	2034.86	1464.2		
		Intermediates		
[i2]	H	D(6)	D(4)	
	513.77	388.29	505.45	
	622.79	510.17	540.45	
	681.45	662.76	606.34	
	734.54	681.42	721.72	
	771.11	768.87	753.26	
	914.84	914.63	799.53	
	963.01	963.01	891.16	
	1106.73	1104.62	1058.42	
	1505.75	1467.04	1475.62	
	2047.43	1513.19	2047.33	
	3164.97	3164.97	2361.63	
	3189.32	3189.32	3177.44	
[i4]	H	D(6)		
	187.18	177.5		
	463.87	423.88		
	623.67	618.03		
	962.26	829.27		
	971.23	874.42		
	1009.72	983.69		
	1276.03	1184.63		
	1381.25	1337.69		
	1562.6	1493.78		
	3086.72	2305.11		
	3099.05	3089.34		
	3174.06	3139.25		
[i1a]	H	D(6)		
	182.59	170.55		
	386.21	321.15		
	583.43	554.52		
	666.95	609.76		
	759.02	669.29		
	832.64	793.47		
	892.62	890.44		
	1134.8	1128.48		
	1555.43	1470.89		
	2044.83	1554.88		
	3128.56	3128.55		
	3208.87	3208.86		
[i1b]	H	D(6)		
	136.02	97.71		
	246.63	243.7		
	560.13	548.85		
	640.34	564.1		
	777.62	664.6		
	897.11	878.18		
	900.42	897.01		
	1139.51	1138.18		
	1577.71	1458.13		
	2026.16	1577.3		
	3088.4	3088.38		
	3191.86	3191.86		
[i1c]	H	D(6)		
	101.15	87.13		
	251.2	247.86		
	537.55	529.82		
	622.59	575.1		
	771.32	646.52		
	857.91	826.82		
	869.32	857.9		
	1111.54	1109		
	1585.53	1456.6		
	2024.51	1584.89		
	2995.98	2995.96		
	3199.56	3199.55		
[i3]	H	D(6)		
	223.74	214.31		
	247.78	243.8		
	604.61	511.26		
	646.34	600.18		
	671.39	647.52		
	677.72	671.08		
	716.51	716.05		
	933.05	834.83		
	2085.74	1584.46		
	2187.43	2085.72		
	2218.54	2203.37		
	3458.46	3458.46		
[i6]	H	D(6)	D(4)	D(2)
	246.32	236.1	231.99	235.09
	272.22	255.69	272.23	257.56
	581.26	499.12	550.13	546.97
	610.08	547.44	582.15	569.74
	687.7	621.52	660.79	674.97
	889.47	888.94	808.03	809.16
	930.08	926.67	829.25	827.8
	1377.95	1377.55	1242.27	1239.08
	1681.84	1484.5	1662.51	1663.53
	2064.41	1681.46	2064.39	2064.39
	3071.09	3071.08	2284.08	2283.29
	3134.59	3134.58	3104.72	3103.97
[i5]	H	D(6)		
	233.95	226.67		
	243.2	235.41		
	589.26	555.24		
	673.08	644.78		
	917.44	788.01		
	1362.01	1252.43		
	1384.75	1258.01		
	1412.58	1405.32		
	1465.01	1460.61		
	2973.03	2188.55		
	3019.48	3001.22		
	3036.9	3035.9		
		Transition States		
[i2–i4]	H	D(6)	D(4)	
	−860.79	−635.61	−860.39	
	338.17	311.16	320.56	
	386.84	385.33	338.77	
	599.13	542.74	533.15	
	670.63	650.33	577.11	
	762.41	743.35	710.06	

Table 4
(Continued)

Species	No Deuterium (cm^{-1})	Deuterated (cm^{-1})		
	871.34	835.89	834.71	
	950.43	935.88	948.14	
	1641.71	1394.55	1582.49	
	1945.09	1638.78	1944.58	
	3218.25	3218.11	2479.05	
	3311.57	3311.53	3225.12	
[i2–i1a]	H	D(6)		
	−414.28	−408.93		
	304.64	296.34		
	392.17	314.47		
	547.46	536.2		
	657.42	552.11		
	751.89	663.31		
	794.03	792.44		
	996.71	985.91		
	1646.98	1476.75		
	2052.32	1646.78		
	3153.75	3153.74		
	3390.82	3390.82		
[i2–i1c]	H	D(6)		
	−182.02	−173.72		
	308.66	247.35		
	546.58	500.65		
	602.83	589.72		
	719.78	633.25		
	810.03	760.85		
	834.39	826.8		
	1057.24	1051.21		
	1568.11	1438.6		
	1999.73	1567.31		
	3026.31	3026.3		
	3231.74	3231.73		
[i2–i3]	H	D(6)		
	−1242.18	−1228.89		
	261.51	250.35		
	345.46	340.81		
	489.38	489.06		
	579.15	560.95		
	632.01	612.1		
	773.93	631.98		
	791.81	710.11		
	1624.08	1484.17		
	1825.68	1626.44		
	2066.96	1825.34		
	3439.77	3439.76		
[i4–i6]	H	D(6)	D(4)	D(2)
	−963.91	−720.18	−957.85	−954.38
	273.24	272.15	262.19	263.01
	359.57	353.59	340.83	341.76
	668.45	608.75	626.72	614.92
	719.74	681.39	653.35	675.13
	789.97	789.87	751.03	751.99
	934.75	933.66	834.92	813.97
	1364.73	1352.44	1227.66	1241.35
	1571.73	1363.42	1550.69	1551.58
	1883.51	1565.58	1883.4	1883.4
	3105.26	3105.14	2317.16	2304.71
	3182.06	3182.06	3138.8	3152.9
[i4–i5]	H	D(6)		
	−1301.2	−1299.6		
	192.21	181.27		
	295.54	291.33		
	367.21	340.19		

Table 4
(Continued)

Species	No Deuterium (cm^{-1})	Deuterated (cm^{-1})
	706.86	685.51
	885.05	813.67
	1028.97	875.37
	1404.89	1319.43
	1456.02	1405.83
	2330.67	2270.12
	3061.15	2334.08
	3146.44	3109.24
[i3–i6]	H	D(6)
	−1789.14	−1357.02
	359.27	324.7
	405.76	378.25
	512.39	509.99
	640.76	635.3
	738.28	695.45
	818.68	782.19
	1019.37	973.58
	1613.18	1180.84
	1737.18	1718.42
	2035.26	2033.72
	3283.36	3283.3
[i6–i1]	H	D(6)
	−1157.44	−1156.69
	163.37	155.77
	280.04	264.98
	304.53	298.69
	322.7	306.78
	519.11	515.03
	666.75	617.34
	804.17	668.43
	1749.96	1463.45
	2034.89	1749.79
	2533.53	2533.48
	3399.9	3399.9
[i6–i5]	H	D(6)
	−886.46	−1054.95
	423.31	528.64
	535.08	580.68
	738.25	624.98
	760.31	871.39
	966.52	1050.15
	1046.44	1123.47
	1276.09	1226.6
	1382.06	1357.27
	1565.31	1515.08
	3015.1	2208.54
	3073.89	3014.03
[i2–p2]	H	D(6)
	−1006.55	−942.64
	283.98	274.49
	437.25	430.19
	498.31	439.85
	670.95	649.15
	801.18	692.39
	846.67	811.46
	1018.42	901.15
	1607.63	1371.43
	1676.37	1673.04
	2091.5	1779.78
	3273.65	3273.63
[i1b–p3]	H	D(6)
	−1238.77	−1163.56
	272.81	265.41

Table 4
(Continued)

Species	No Deuterium (cm^{-1})	Deuterated (cm^{-1})
	285.84	280.76
	496.96	495.79
	566.62	545.44
	632.36	596.69
	708.29	708.1
	1070.42	847.99
	1633.58	1280.45
	1853.66	1685.76
	1967.01	1960.41
	3452.36	3452.35
[i3–p3]	H	D(6)
	−1438.85	−1210.32
	225.17	216.49
	249.42	244.91
	589.93	507.09
	627.63	607.12
	658.26	657.71
	737.44	694.1
	741.7	737.46
	1594.7	1289.3
	1809.43	1607.19
	2062.75	2062.69
	3456.06	3456.06
[i5–p3]	H	D(6)
	−1469.32	−1457.52
	143.8	127.34
	196.93	189.97
	292.05	278.92
	680.58	677.73
	694	689
	832.3	787.39
	1072.24	1033.82
	1321.39	1063.62
	1682.8	1641.36
	3030.55	2458.86
	3298.07	3030.2
	Products	
[p1]	H	D(4)
	667.06	587.97
	698.11	594.35
	762.19	737.76
	895.32	791.15
	1000.12	926.78
	1105.91	1054.98
	1494.73	1464.78
	3156.35	2354.39
	3180.27	3168.6
[p2]	H	D(2)
	582.86	516.79
	670.43	596.22
	757.38	653.09
	849.61	721.9
	1597.54	1542.92
	3219.6	2410.62
[p3]	H	D(2)
	169.08	159.58
	262.22	249.41
	514.6	403.39
	618.21	610.21
	772.51	610.36
	1963.62	1855.39
	3448.09	2639.95

Table 4
(Continued)

Species	No Deuterium (cm^{-1})	Deuterated (cm^{-1})
	Higher Energy Structures	
[i7]	H	D(6)
	70.37	69.83
	77.36	76.04
	626.85	520.3
	640.62	626.62
	654.64	628.18
	945.93	809.8
	948.74	871.74
	953.05	948.35
	2137.41	1612.85
	2223.1	2137.44
	2241.65	2223.38
	2245.96	2243.71
[p6] (H Loss)	H	D(4)
	298.68	271.6
	351.02	298.65
	580.31	532.68
	745.38	632.8
	777.32	743.16
	810.87	787.57
	1764.64	1399.35
	1946.43	1764.77
	3376.62	3376.85
[p10] (H Loss)	H	D(4)
	286.75	242.44
	300.27	300.13
	671.78	553.46
	784.78	699.69
	799.81	794
	1052.17	946.5
	1872.51	1615.82
	2238.06	1872.77
	2251.23	2244.72
[p4] (H Loss)	H	D(4)
	200.87	197.22
	266.66	253.06
	749.25	727.91
	996.43	880.31
	1016.61	901.73
	1432.54	1299.03
	1730.63	1713.3
	3057.49	2273.36
	3116.33	3088.31
[p5] (H Loss)	H	D(4)
	184.63	181.27
	252.6	240.77
	602.02	579.6
	630.11	629.76
	780.45	653.39
	829.71	780.41
	2053.01	1477.05
	2060.25	2060.24
	3452.32	3452.33
[p7] (H Loss)	H	D(4)
	117.29	116.96
	144.57	139.93
	670.84	562.24
	674.25	597.28
	796.14	789.09
	997.79	902.96
	1958.75	1634.15

Table 4
(Continued)

Species	No Deuterium (cm^{-1})	Deuterated (cm^{-1})
	2259.2	1959.05
	2282.12	2270.92
[p11] (H Loss)	H	
	82.38	
	192.97	
	693.85	
	810.87	
	831.9	
	943.28	
	1395.32	
	3117.23	
	3211.55	
[p9] (H_2 Loss)	H	D(2)
	118.8	89.25
	219.42	214.49
	690.84	514.64
	765.43	761.34
	1823.92	1475.57
	2048.53	1823.77
[p8] (H_2 Loss)	H	D(2)
	134.74	123.71
	160.69	153.41
	597.31	459.64
	759.36	751.12
	1876.35	1504.78
	2090.97	1877.31

Notes. For each molecule, isotopomers are indicated by specifying the hydrogen atom replaced by deuterium. For instance, D(3) represents the isotopomer obtained by replacing the hydrogen at the third heavy atom with deuterium. Atom numbers correspond to the nuclear geometries provided in Table 3. Imaginary frequencies are identified by a negative sign. Frequencies are obtained from B3LYP/6-311+G** calculations.

Consequently, we have to conclude that the molecular hydrogen loss channel is—as confirmed experimentally—closed. Here, the experimentally determined reaction energy to form products of 54 amu (SiC_2H_2/SiC_2D) plus 2 amu (D/H_2) of 13 ± 8 kJ mol^{-1} only correlates with the computed reaction energy to form silacyclopropenylidene (c-SiC_2H_2) [p1] plus atomic deuterium (−10 kJ mol^{-1}), and not with the pathway leading to the D1-silapropenylidyne radical (DCCSi) [p3] plus molecular hydrogen (H_2) (−62 kJ mol^{-1}). Considering the hydrogen deuteride (HD) emission, the energetics suggest that intermediates [i1] to [i3] and [i5] might lose hydrogen deuteride in overall exoergic reactions (37–62 kJ mol^{-1}). However, intermediate [i1] undergoes de facto barrierless isomerization to [i2] rather than losing hydrogen deuteride via a tight exit transition state located 15 kJ mol^{-1} above the separated products. Furthermore, the transition states involved in the hydrogen deuteride emission from intermediates [i2] and [i5] are located at 82 and 103 kJ mol^{-1}, respectively, above the separated products and are energetically not accessible. Lastly, the hydrogen deuteride loss from intermediate [i3] is energetically less favorable compared to the back reaction of [i3] to [i1] followed by atomic deuterium loss of the latter. In order for molecular "hydrogen" elimination to occur, significant time would need to be spent at either [i1] or [i3]. As the [i1] to [i2] transition is virtually barrierless, it is not likely that the [i1] will exist long enough to collect sufficient energy (+15 kJ mol^{-1}) in the proper vibrational modes to eject molecular "hydrogen." Therefore, we can conclude that the hydrogen deuteride elimination should not be observable, an observation that is in line with the experimental results.

To summarize, our ab initio calculations suggest the following for the reaction of the D1-silylidyne radical with acetylene. First, both the molecular hydrogen (H_2) and the hydrogen deuteride (HD) elimination channels are closed due to the high energy of the associated transition states. Second, the calculated energetics suggest both the atomic hydrogen and deuterium atom elimination channels are nominally open based on barrier heights that permit isotope scrambling. However, only the latter is realized experimentally, evidently reflecting non-statistical dynamics involved in the decomposition of intermediate [i2].

5. REACTION MECHANISM AND CHEMICAL DYNAMICS

We are now combining our experimental findings with the results from the ab initio calculations to propose the underlying reaction mechanism(s) and the chemical dynamics of the reaction. The reaction of the D1-silylidyne radical with acetylene proceeds via indirect scattering dynamics and is initiated by addition of D1-silylidyne to one or two carbon atoms of the acetylene molecule forming collision complexes [i1] and [i2], respectively. The indirect scattering dynamics were verified by the shape of the CM angular distribution depicting intensity over the complete scattering range from 0° to 180°. Further, the computations indicate that these reactions involve no entrance barriers. Complex formation is therefore dictated by long-range attractive forces. Reactions with small impact parameters should lead preferentially to 1-sila-1-propene-1,3-diylidene [i1], whereas large impact parameters are expected to result in formation of the 1-silacyclopropenyl radical [i2]. Considering the energy of the transition states, intermediate [i1] is expected to undergo preferential ring closure via a barrier of less than 1 kJ mol^{-1} to intermediate [i2]. The combination of this low barrier transition with the energy gained by the formation of the silicon–carbon bond(s) upon association results in a fluxional geometry in which [i1] and [i2] are constantly interconverting. Intermediate [i2] fragments via a loose exit transition state through atomic deuterium loss forming the silacyclopropenylidene (c-SiC_2H_2) molecule [p1] in an overall exoergic reaction (−10 kJ mol^{-1}). The loose nature of the transition state was also verified experimentally based on the CM translational energy distribution peaking close to zero translational energy. The barrierless nature of the reversed reaction of the deuterium atom addition to the closed shell silacyclopropenylidene molecule (c-SiC_2H_2; X^1A_1) is surprising as hydrogen atom additions to closed shell molecules are associated with entrance barriers of typically 5–30 kJ mol^{-1}. However, the ring bonding in silacyclopropenylidene is unique and best rationalized as a combination of the Dewar–Chatt–Duncanson model plus some delocalization of the out-of-plane carbon–carbon π electrons into the empty p orbital of the silicon atom. Therefore, the deuterium atom can add without barrier to the empty silicon p-type orbital of silacyclopropenylidene. Finally, both experiments and computations agree that only the atomic deuterium loss is open; competing exit channels involving molecular hydrogen and hydrogen deuteride losses are closed. Thus, under our experimental conditions, the reaction of the D1-silylidyne radical with acetylene leads solely to the silacyclopropenylidene molecule (c-SiC_2H_2) plus atomic deuterium in a slightly exoergic reaction (−10 kJ mol^{-1}).

6. ASTROPHYSICAL IMPLICATIONS AND CONCLUSIONS

Having uncovered a facile formation route of the silacyclopropenylidene molecule (c-SiC_2H_2) under single-collision conditions, we will now discuss the implications of this discovery to the "real" ISM. Our combined experimental and computational study exposed a barrierless and exoergic route to form silacyclopropenylidene under single-collision conditions via the gas phase reaction of the D1-silylidyne radical with acetylene with all isomerization barriers located below the energy of the separated reactants. When considering the competing reaction channels such as hydrogen abstraction or the formation of higher energy SiC_2H_2 isomers like silavinylidenecarbene (H_2CCSi), we can conclude that the silacyclopropenylidene molecule (c-SiC_2H_2) represents the sole reaction product formed in circumstellar envelopes close to the central star. Hence, the bimolecular collision of the simplest silicon-bearing radical silylidyne (SiH) with omnipresent acetylene (C_2H_2) can be considered as a prototype mechanism leading to the formation of organosilicon molecules in circumstellar envelopes. Recall that we conducted the reaction with D1-silylidyne to elucidate the position of the atomic hydrogen loss. However, in the "real" ISM, the silylidyne radical (SiH) rather than the D1-silylidyne radical reacts with acetylene. This reaction was computed to be slightly more exoergic, i.e., -13 kJ mol^{-1}, to form the silacyclopropenylidene molecule plus atomic hydrogen. Acetylene would therefore be effectively tied to the synthesis of organosilicon species as the main carbon reservoir in carbon-rich outflows. Our investigation also serves as a proof-of-concept study highlighting that hitherto poorly studied reactions of silylidyne radicals with more complex hydrocarbons such as ethylene (C_2H_4) and substituted acetylenes/olefines could significantly advance circumstellar organosilicon chemistry.

Once formed, the organosilicon molecules might be photolyzed easily; pioneering laboratory studies by Maier et al. provided compelling evidence that photolysis of silacyclopropenylidene (c-SiC_2H_2) yields the cyclic silicon dicarbide molecule (c-SiC_2) (Maier et al. 1995b). This finding has important implications. Chemical models for the carbon-rich star IRC+10216 (Cherchneff 2012) produce fractional abundances of silicon dicarbide (c-SiC_2) of some 5×10^{-8}, when the chemical effects of shocks are included in the models. Here, silicon dicarbide is proposed to be formed through reactions between silicon carbide (SiC) molecules; however, other formation routes were not considered. Recent observations of silicon dicarbide with Herschel/HIFI (Cernicharo et al. 2010) indicate a similar but somewhat higher abundance of 2×10^{-7}. The reaction of silylidyne (SiH) with acetylene (C_2H_2) leading to silacyclopropenylidene (c-SiC_2H_2) could be an important first step toward silicon dicarbide (c-SiC_2) in these environments, as silacyclopropenylidene (c-SiC_2H_2) could easily undergo collisional cleavage of the carbon–hydrogen bonds in the warm post-shock gas or even through photolysis. Our findings, that an organosilicon molecule forms via reaction of silylidyne with acetylene, present a strong alternative to previously postulated reactions leading to silicon-bearing molecules via reactions involving atomic silicon. Kinetics studies suggest that at temperatures down to 15 K, ground-state silicon atoms react fast with acetylene with rate constants of a few $\times 10^{-10}$ cm^3 s^{-1} (Basu & Husain 1988; Canosa et al. 2001). Smith et al. proposed that at these low temperatures, intersystem crossing operates efficiently, and the spin-forbidden exoergic molecular hydrogen loss channels to c-SiC_2 plus molecular hydrogen are open (Smith et al. 2006). However, at elevated temperatures close to the photosphere of carbon stars, intersystem crossing is rather inefficient, and c-SiC_2 cannot be formed via the bimolecular reaction of silicon atoms with acetylene (Kaiser & Gu 2009). However, c-SiC_2 can be synthesized upon photolysis and in shocked regions through hydrogen loss from silacyclopropenylidene (c-SiC_2H_2), which in turn can be generated through bimolecular reactions of silylidyne (SiH) with acetylene (C_2H_2) as demonstrated in the present work.

To conclude, the pathways involving silacyclopropenylidene (c-SiC_2H_2) may provide the key to understanding the high abundance of solid-phase silicon carbide in the harsh environment of the ISM, where the destruction via sputtering and interstellar shocks is rapid. Our study delivers compelling evidence that small organosilicon molecules such as silacyclopropenylidene can be formed via facile, barrierless reactions involving the simplest silicon-bearing radical (silylidyne) and acetylene. These reactions could supply the molecular feedstock of organosilicon molecules necessary to account for the ubiquitous presence of interstellar silicon-carbide grains via a "bottom up" synthesis starting with small silicon-bearing precursor molecules as proposed here. Since the reaction is barrierless and all transition states involved are located below the energy of the separated reactants, exoergic processes of this reaction class could be highly relevant for chemical growth of silicon-carbide dust grains in the low temperature conditions of the ISM. Dust destruction is very rapid in the ISM even for such refractory solids as silicon carbide (Jones et al. 1994). While grain growth in the ISM is often invoked to reconcile the large discrepancy of injection and destruction timescales with the observed high abundance of interstellar dust (Draine 2009), chemical routes have never been identified. Even first-order questions such as whether silicon-carbide dust grows an "SiC mantle" in the ISM or a silicate oxide mantle have not been addressed. The reaction route proposed here opens up a "homogeneous" silicon-carbide growth on silicon-carbide grains in the ISM. Finally, although silicon dicarbide (c-SiC_2) has been detected in the circumstellar envelope of IRC+10216, silacyclopropenylidene has escaped astronomical detection. The difficulty in observing silacyclopropenylidene might be due to poorly characterized rotational spectra in the laboratory, inaccurate rotational constants, or simply a lifetime too short due to photolysis, shocks, or grain growth. Therefore, prospective searches for silacyclopropenylidene utilizing the Atacama Large Millimeter Array (ALMA) combined with novel astrochemical models are expected to provide critical constraints and a comprehensive picture of the basic molecular processes involved in the formation of organosilicon molecules and their link to silicon-carbide grain formation in the ISM.

This work at the University of Hawaii was supported by the U.S. National Science Foundation (CHE-0948258). N.J.M. thanks Narbe Mardirossian for insightful discussions. Studies of interstellar chemistry at Leiden Observatory are supported through advanced-ERC grant 246976 from the European Research Council, through a grant by the Dutch Science Agency, NWO, as part of the Dutch Astrochemistry Network, and through the Spinoza premie from the Dutch Science Agency, NWO.

REFERENCES

Basu, S. C., & Husain, D. 1988, J. Photochem. Photobiol. A, 45, 141
Bauer, W., Becker, K. H., Dueren, R., Hubrich, C., & Meuser, R. 1984, CPL, 108, 560

Canosa, A., Le Picard, S. D., Gougeon, S., et al. 2001, JChPh, 115, 6495
Cernicharo, J., Ceccarelli, C., Nisini, B., et al. 2010, A&A, 521, L1
Cherchneff, I. 2006, A&A, 456, 1001
Cherchneff, I. 2012, A&A, 545, A12
Cherchneff, I., Le Teuff, Y. H., Williams, P. M., & Tielens, A. G. G. M. 2000, A&A, 357, 572
Decin, L., Cherchneff, I., Hony, S., et al. 2008, A&A, 480, 431
Draine, B. T. 2009, in ASP Conf. Ser. 414, Cosmic Dust: Near and Far, ed. T. Henning, E. Grün, & J. Steinacker (San Francisco, CA: ASP), 453
Dunning, T. H., Jr. 1989, JChPh, 90, 1007
Fernandez, I., Duvall, M., Wu, J. I. C., Schleyer, P. v. R., & Frenking, G. 2011, Chem. Eur. J., 17, 2215
Halkier, A., Helgaker, T., Jorgensen, P., et al. 1998, CPL, 286, 243
Jones, A. P. 2001, RSPTA, 359, 1961
Jones, A. P., Tielens, A. G. G. M., Hollenbach, D. J., & McKee, C. F. 1994, ApJ, 433, 797
Kaiser, R. I., & Gu, X. 2009, JChPh, 131, 104311
Kaiser, R. I., Maksyutenko, P., Ennis, C., et al. 2010, FaDi, 147, 429
Kong, J., White, C. A., Krylov, A. I., et al. 2000, JCoCh, 21, 1532
Maier, G., Pacl, H., & Reisenauer, H. P. 1995a, Angew. Chem. Int. Ed., 34, 1439
Maier, G., Pacl, H., Reisenauer, H. P., Meudt, A., & Janoschek, R. 1995b, JAChS, 117, 12712
Maier, G., Reisenauer, H. P., & Egenolf, H. 1998, Eur. J. Org. Chem., 1998, 1313
Maier, G., Reisenauer, H. P., & Pacl, H. 1994, Angew. Chem., 106, 1347
Millar, T. J., & Herbst, E. 1994, A&A, 288, 561
Millar, T. J., Herbst, E., & Bettens, R. P. A. 2000, MNRAS, 316, 195
Ohishi, M., Kaifu, N., Kawaguchi, K., et al. 1989, ApJL, 345, L83
Pople, J. A., Head-Gordon, M., & Raghavachari, K. 1987, JChPh, 87, 5968
Redman, M. P., Viti, S., Cau, P., & Williams, D. A. 2003, MNRAS, 345, 1291
Smith, I. W. M., Sage, A. M., Donahue, N. M., Herbst, E., & Quan, D. 2006, FaDi, 133, 137
Speck, A. K., Barlow, M. J., & Skinner, C. J. 1997, M&PS, 32, 703
Srinivas, R., Suelzle, D., Weiske, T., & Schwarz, H. 1991, IJMSI, 107, 369
Su, M. D., Amos, R. D., & Handy, N. C. 1990, JAChS, 112, 1499
Talbi, D. 2005, CP, 313, 17
Thaddeus, P., Cummins, S. E., & Linke, R. A. 1984, ApJL, 283, L45
Tielens, A. G. G. M. 1998, ApJ, 499, 267
Vacek, G., Colegrove, B. T., & Schaefer, H. F., III. 1991, JAChS, 113, 3192
Van Orden, A., Provencal, R. A., Giesen, T. F., & Saykally, R. J. 1995, CPL, 237, 77
Vernon, M. 1981, PhD thesis, Univ. California, Berkley
Wakelam, V., Smith, I. W. M., Herbst, E., et al. 2011, SSRv, 156, 13
Weis, M. S. 1986, PhD thesis, Univ. California, Berkley
Willacy, K., & Cherchneff, I. 1998, A&A, 330, 676
Yasuda, Y., & Kozasa, T. 2012, ApJ, 745, 159
Zinner, E. 1998, M&PS, 33, 549
Ziurys, L. M. 2006, PNAS, 103, 12274